JOURNAL OF MATERIALS SCIENCE 27 (1992) 1505–1513

Stress relaxation in bending of type AISI 304 stainless steel at 773 and 823 K

F. POVOLO*
International Centre for Theoretical Physics, Trieste, Italy
R. J. TINIVELLA, J. F. REGGIARDO, G. B. BOTTERI
Universidad Tecnologica Nacional, Facultad Regional San Nicolas, CC118-2900 San Nicolas, Argentina

Stress relaxation measurements at 773 and 823 K in bending and for different initial stresses in type AISI 304 stainless steel are reported. Several thermal treatments were given to the specimens prior to the relaxation testing. The data are fitted to a general equation that describes thermally activated dislocation motion and it is shown that, in some cases, the internal stress changes with the applied stress. No substantial differences were found in the stress relaxation behaviour on changing the thermal treatment. This is attributed to the influence of dynamic strain ageing; an equation which can be used to describe experimental log stress against log strain rate curves is presented.

1. Introduction

Only limited data are available in the literature on the stress relaxation behaviour of stainless steels. Conway *et al.* [1] have reviewed the stress relaxation behaviour of stainless steels for data analysed in a stress against time diagram. Rhode and Swearengen [2] considered the load relaxation data reported by Conway [3], for 304 and 316 stainless steels during cyclic deformation and various holding times, for experiments conducted at 923 and 811 K. The stress relaxation curves were analysed in a stress against strain-rate diagram by using the relationship

$$\dot{\varepsilon}/\dot{\varepsilon}_1 = (1 - S)[(\sigma - \sigma_i)/\sigma_1]^{m/n} + S[(\sigma - \sigma_i)/\sigma_1]^n \quad (1)$$

where σ is the applied stress, $\dot{\varepsilon}$ the plastic strain rate, m is a state variable that relates dislocation velocity to stress, n is a state variable that denotes the recovery rate, the state parameter σ_i is an internal stress which becomes zero at high temperatures, and S is a functional relationship between m, n, strain hardening and recovery. σ_1 and $\dot{\varepsilon}_1$ are the stress and strain rate, respectively, at the beginning of the relaxation. Equation 1 can give either concave upward, linear or concave downward curves.

The state variable approach proposed by Hart [4, 5] has been used by several authors [6–13] to describe the load relaxation behaviour of type 304 and type 316 stainless steels. Hart's phenomenological model essentially consists of two parallel branches. At high homologous temperatures, the constant hardness log σ–log $\dot{\varepsilon}$ stress relaxation curves are described by

$$\ln(\sigma^*/\sigma) = (\varepsilon^*/\varepsilon)^\lambda \quad (2)$$

where σ^* is the hardness, λ is a temperature-independent parameter, and $\dot{\varepsilon}^*$ depends on temperature, heat treatment and deformation. Equation 2 describes concave downward log σ–log $\dot{\varepsilon}$ curves, and the rate of deformation in the region where this equation applies is assumed to be controlled by diffusive processes.

The branch which is important at low homologous temperature gives the constant hardness log σ–log $\dot{\varepsilon}$ curves described by

$$\dot{\varepsilon} = Q(\sigma_f/G)^M \quad (3)$$

where G is the shear modulus, Q is a rate parameter and is moderately temperature dependent compared with $\dot{\varepsilon}^*$, σ_f is an effective stress and is $(\sigma-\sigma^*)$ in the region where deformation processes represented by Equation 2 are not important, and M is a constant. Equation 3 leads to concave upward or linear log σ–log $\dot{\varepsilon}$ curves, and it is assumed to result from dislocation glide controlled processes.

In the intermediate temperature range, deformation processes represented by both Equations 2 and 3 will be important. In this range, both branches of the phenomenological model will be operative such that

$$\sigma = \sigma^* \exp[-(\dot{\varepsilon}^*/\dot{\varepsilon})^\lambda] + G(\dot{\varepsilon}/Q)^{1/M}. \quad (4)$$

Most of the data were obtained at room temperature and have been interpreted in terms of Equation 3. Moreover, it was found that the parameters of Equation 3 were dependent on the prior thermomechani-

* *Permanent address* Comisión Nacional de Energia Atómica, Departamento de Ciencia de los Materiales, Av. del Libertador 8250, (1429) Buenos Aires, Argentina and Departamento de Fisica, Facultad de Ciencias Exactas y Naturales, Universidad de Buenos Aires, Pabellon 1, Ciudad Universitaria, (1428) Buenos Aires, Argentina.

0022–2461

cal treatment given to the specimens [6, 9]. The measurements in type-316 stainless steel were extended to higher temperatures [11, 13] and could be described by Equation 4 up to a temperature of the order of 773 K. Microstructural changes were observed above this temperature. A grain-boundary sliding contribution to the relaxation curves was observed at 873 K in highly stabilized type-316 stainless steel [13]. This contribution was described by an equation similar to Equation 2 with $\lambda = 0.32$.

Anciaux [14] has published load relaxation data near 563 K for three austenitic stainless steels. The tests were conducted in a strain-controlled servo-hydraulic test machine near the yield point strain levels. For stainless steel type AISI 304, Anciaux reported the log σ–log $\dot{\varepsilon}$ curves, at different strain levels, for mill-annealed specimens. The shape of the log σ–log $\dot{\varepsilon}$ stress relaxation curves was found to depend on the strain level, but no explanation was given by the author for this behaviour. Povolo and Tinivella [15], however, have interpreted these data in terms of a general expression that describes the stress relaxation behaviour as a thermally activated process

$$\dot{\varepsilon} = \dot{\varepsilon}_1 \exp[-\Delta G(\bar{\sigma})/kT] \quad (5)$$

where $\dot{\varepsilon}_1$ is a general pre-exponential factor, T is the absolute temperature, k is Boltzmann's constant, ΔG is the change in free enthalpy and $\bar{\sigma}$ is the effective stress, that is, $\bar{\sigma} = \sigma - \sigma_i$. In different regions of the stress against strain-rate curves, Equation 5 was reduced to particular expressions like Equations 2 and 3, which allow a determination of the physical parameters involved, such as internal stress, activation volume, etc.

Povolo and Tinivella [16] have reported stress relaxation data, in bending and at 773 K, of type 304 stainless steel. Four different thermomechanical treatments were given to the specimens prior to the stress relaxation experiments, and the measurements were extended up to times of the order of 450 h at various initial stresses. The shapes of the log σ – log $\dot{\varepsilon}$ curves were found to be strongly dependent on the previous thermomechanical treatment, and were interpreted in terms of a stress-partitioned power law, of the type of Equation 3, with either a constant or a variable internal stress. In fact, this stress-partitioned power law and Equation 2 are particular cases of Equation 5. Moreover, several activation parameters were obtained from the stress relaxation curves.

It is the purpose of this paper to present additional data on the stress relaxation, in bending and at 773 and 823 K, of type 304 stainless steel. The measurements at 773 K were extended up to times of the order of 180 h, in specimens with new thermomechanical treatments, and those at 823 K were extended up to times of the order of 3000 h. Finally, the influence of the different treatments on the shape of the stress relaxation curves will be discussed and the different activation parameters will be analysed in detail.

2. Experimental procedure

2.1. Specimen preparation

The original material was supplied in the form of a sheet 0.52 mm thick and in mill-annealed conditions. The typical composition of the alloy is given elsewhere [16]. The specimens were prepared with the axis parallel to the rolling direction and, in addition to the as-received condition, four different thermal treatments were used prior to the stress relaxation measurements. In fact, the specimens (8 mm wide and 98 mm long) were carefully cleaned and sealed into fused silica tubes with argon atmosphere. These tubes were heated for 1 h at 1323, 1255 or 1172 K, and dropped into oil for a quenching treatment. Part of the specimens, heated at 1323 K, were heat-treated into a fused silica tube connected to a high-vacuum equipment, at 993 K for 16 h, and subsequently cooled by removing the furnace (air cooling). These different thermal treatments are named 0, A, B, C and D, respectively, as indicated in Table I. The microhardness of each specimen, obtained after the different thermal treatments, and the average grain size, as measured after the stress relaxation tests, are indicated in the same table.

TABLE I Thermal treatments given to specimens and microhardness (prior to stress relaxation tests) and average grain size (after stress relaxation tests)

Thermal treatment	Name	Microhardness (H_V)	Grain size (μm)
As-received	0	182	22
0 + 1 at 1323 K in argon and oil-quenched	A	180	90
0 + 1 h at 1255 K in argon and oil-quenched	B	164	53
0 + 1 h at 1172 K in argon and oil-quenched	C	179	22
0 + A + 16 h at 993 K in vacuum and air cooled	D	170	94

2.2. Stress relaxation measurements

The specimens, originally flat, were bent into stainless steel holders with radii which gave maximum outer fibre stresses, under elastic bending, between approximately 120 and 320 MPa. The holders are similar to those described by Fraser *et al.* [17]. The holders with the specimens were inserted into a furnace either at 773 or 823 K, and extracted periodically for curvature measurements. The temperature was controlled with thermocouples attached to the holder near the specimens and the fluctuations were of the order of $\pm$ 1 K. The radii of curvature, R_i, after releasing the specimens from the holders, were determined by measuring the coordinates of different points with respect to a reference plane, in the arc of circumference determined by the curved beam, and feeding the data to a computer programme which calculated the average radius by a least square fitting. Duplicate specimens were used in order to observe the dispersion between equivalent specimens in the results. The stresses at the surface of the beam, σ_0, before unloading were determined by using the relationship [18, 19]

$$\sigma = 2/3\,\sigma_b + \Sigma/3(d\sigma_b/d\Sigma) \quad (6)$$

where

$$\sigma_b = Eh/2(1/R_i - 1/R) \quad (7)$$

is the measured stress change at the surface of the bent specimen, after releasing it from the holder; h is the thickness of the specimen; R is the radius of curvature of the holder; and E is Young's modulus (168 GPa at 773 K and 163 GPa at 823 K [20]). The initial stress, Σ, at the surface of the bent specimen was not obtained from the relationship $\Sigma = Eh/2R$ since some plastic deformation was observed in the specimens during bending into the holders. In this situation, it was more reliable to take for Σ the value of σ_b obtained from each σ_b against-time curve by an extrapolation to the origin.

3. Results

Figs 1 and 2 show the measured stress change at the surface of the specimens as a function of time, at 773 and 823 K, respectively. The curves corresponding to the different types of specimens and the initial stresses employed are also indicated in these figures. Each curve corresponds to the average value obtained from two specimens and the data have been disposed in the way shown in Figs 1 and 2 to avoid superpositions. The stresses, σ, at the surface of the specimens before unloading, which correspond to the values that would be obtained in the same material under initial uniaxial stresses given by Σ, can be calculated by using Equation 6. In fact, average curves were drawn through the

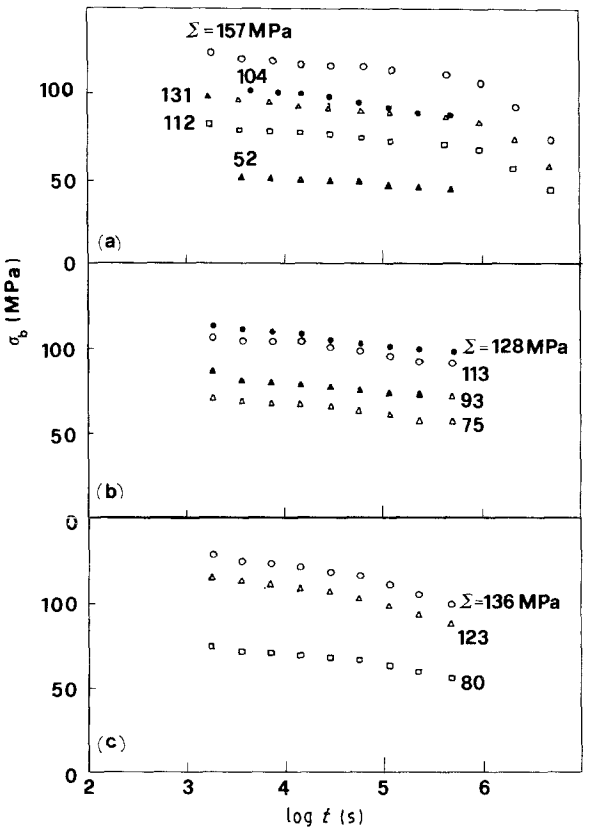

Figure 1 Measured stress change at the surface as a function of time at 773 K. (a) Full symbols, type A; open symbols, type O specimens. (b) Open symbols, type B; full symbols, type D. (c) Type C. Corresponding initial stresses are given on each curve.

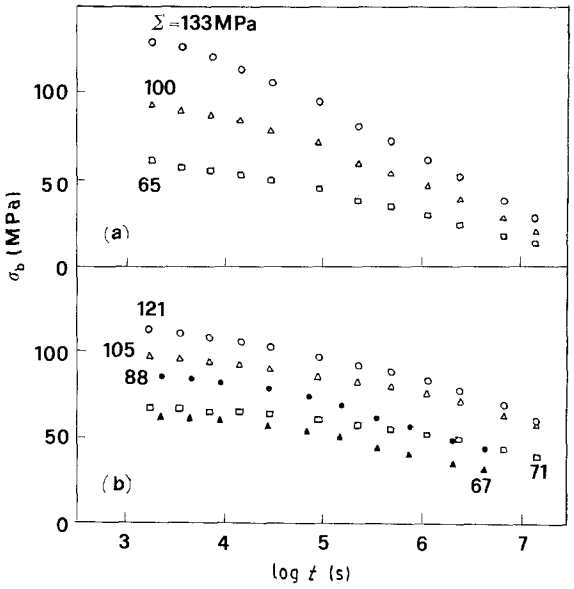

Figure 2 Measured stress at the surface as a function of time at 823 K. (a) Type C; (b) full symbols, type B; open symbols, type D specimens. Corresponding initial stresses are given on each curve.

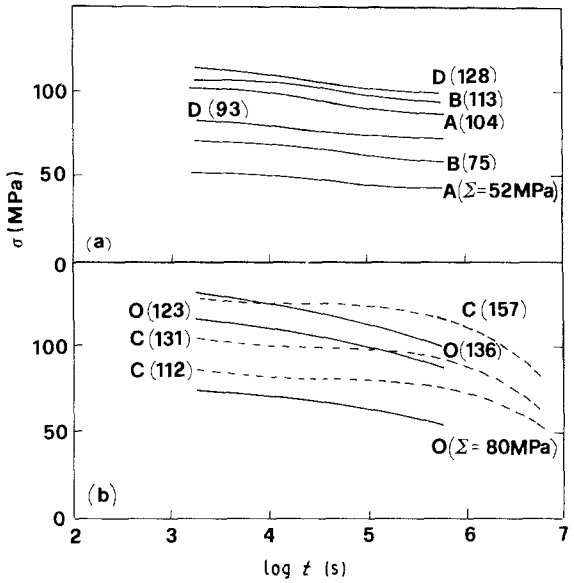

Figure 3 Stress at surface of specimen before unloading as a function of time at 773 K. (a) Type of specimen and the initial stress are indicated on each curve. (b) Full curves correspond to type C; broken curves to type O specimens.

data points of Figs 1 and 2, and σ was calculated from these curves. The σ against log t curves obtained in this way are shown in Figs 3 and 4. Once σ is known, the stress against strain-rate curves can be obtained by differentiating the curves of Figs 3 and 4, as $\dot{\varepsilon} = -\dot{\sigma}/E$. The log stress against log strain-rate relaxation curves are shown in Fig. 5 for 773 K, and in Fig. 6 for 823 K. It is seen that the shape of these curves depends on the thermal treatment and on the testing temperature. Furthermore, there are mainly, three types of curves: concave upward, concave downward, or mixed. Thus a procedure described in detail elsewhere [15, 16, 21] will be used to describe the log $\dot{\sigma}$ − log $\dot{\varepsilon}$ curves of Figs 5 and 6. Briefly, it will be assumed that these curves are described by Equation

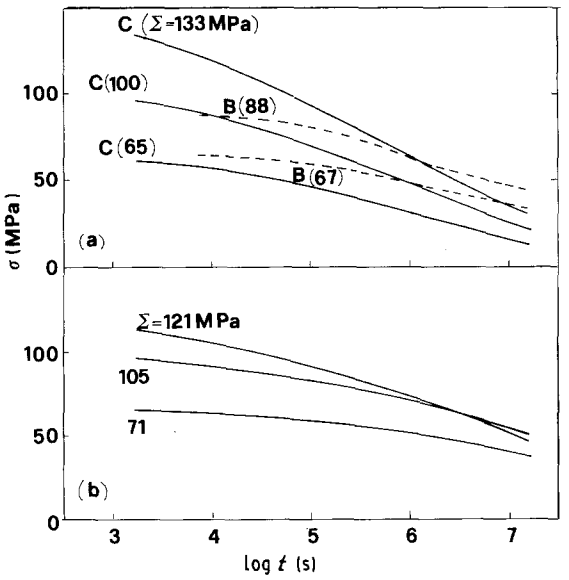

Figure 4 Stress at surface of specimen before unloading as a function of time at 823 K. (a) Full curves correspond to type C; broken curves to type B specimens; (b) type D. Corresponding initial stresses are indicated on each curve.

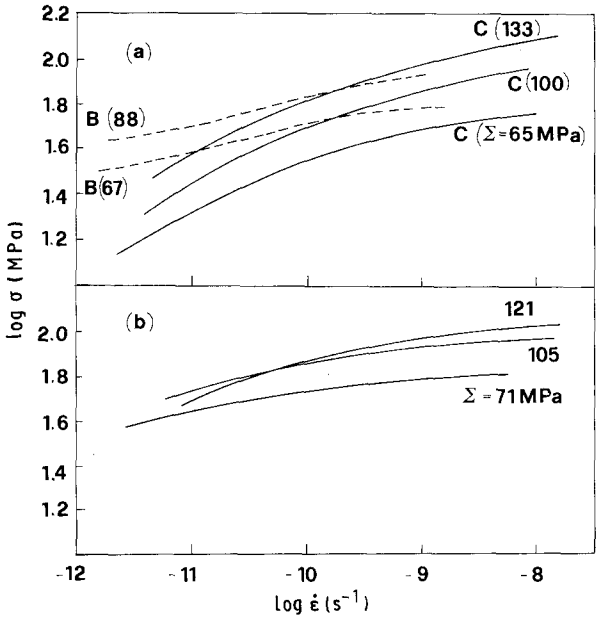

Figure 6 Stress against rate relaxation curves, at 823 K, for specimens shown in Fig. 4. (a) Broken curves, type B; full curves, type C specimens; (b) type D. Corresponding initial stresses indicated on each curve.

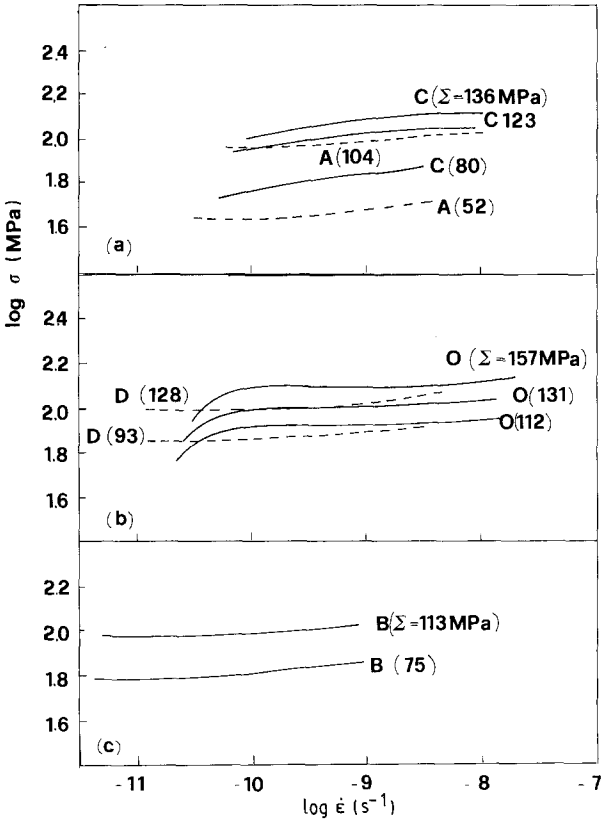

Figure 5 Stress against strain rate relaxation curves, at 773 K, for specimens shown in Fig. 3. (a) Broken curves, type A; full curves, type C specimens. (b) Broken curves type D; full curves, type O (c) Type B. Corresponding initial stresses indicated on each curve.

5, written as

$$\dot{\varepsilon} = \dot{\varepsilon}_0 \exp[-\Delta G^m(\bar{\sigma})/kT] \quad (8)$$

where $\Delta G^m(\bar{\sigma})$ gives the contribution to the change in the free enthalpy due to the applied stress.

Furthermore, the Johnston–Gilman [22] equation

$$\dot{\varepsilon} = \phi\rho v_0 \left(\frac{\bar{\sigma}}{\sigma_0}\right)^{m^*} = \dot{\varepsilon}_{J-G}\left(\frac{\bar{\sigma}}{\sigma_0}\right)^{m^*} \quad (9)$$

with

$$\dot{\varepsilon}_{J-G} = \phi\rho b v_0 \quad (10)$$

where ϕ is an orientation factor, ρ is the mobile dislocation density, b is the Burgers vector and v_0, σ_0 and m^* are material constants, can be written in the form of Equation 8 if

$$\Delta G^m(\bar{\sigma})|_{J-G} = m^* kT \ln(\bar{\sigma}/\sigma_0) \quad (11)$$

and

$$\dot{\varepsilon}_0 = \phi\rho b v_0 = \dot{\varepsilon}_{J-G} \quad (12)$$

It should be pointed out that Equation 9 is equivalent to Equation 3. Moreover, Equation 2 can be written in the form of Equation 8 if

$$\Delta G^m(\bar{\sigma})|_H = -\left(\frac{kT}{\lambda}\right)\ln[\ln(\sigma^*/\sigma)] \quad (13)$$

and

$$\dot{\varepsilon}_0 = \dot{\varepsilon}^* \quad (14)$$

Equation 9 reduces to equation 2 if the internal stress changes according to the law

$$\sigma_i = \sigma - \sigma_0[\ln(\sigma^*/\sigma)]^{-1/\lambda m^*} \quad (15)$$

for $\sigma < \sigma^*$

The activation volume, defined by

$$V^* = -\partial\Delta G^m(\bar{\sigma})/\partial\bar{\sigma}|_T \quad (16)$$

in the case of the Johnston–Gilman equation reduces to

$$V^* = kTm^*/\bar{\sigma} \quad (17)$$

and, in the case of Hart's equation (Equation 2) to

$$V^* = \frac{m^* kT}{\sigma_0}[\ln(\sigma^*/\sigma)]^{1/\lambda m^*} \quad (18)$$

Then, when the representation of log σ against log $\dot{\varepsilon}$ curves is linear or shows upward curvature, Equation 8 reduces to Equation 9 and the data are described by the Johnston–Gilman equation. If the curves show a downward curvature, Equation 8 reduces to Equation 2, and the data are described by Hart's equation for high homologous temperatures, or by the equivalent, the Johnston–Gilman equation with an internal stress that varies with the applied stress according to Equation 15. Finally, in the case of mixed curvature, there will be a transition region where the experimental curve changes curvature, that is, where the data can be described by both Equations 2 and 9. Furthermore, in the transition region

$$\Delta G^m(\bar{\sigma})|_{J-G} = \Delta G^m(\bar{\sigma})|_H \quad (19)$$

$$\dot{\varepsilon}_H = \dot{\varepsilon}_{J-G} \quad (20)$$

and on equating Equations 17 and 18 it is easy to show that at the critical stress, σ_c, that

$$\sigma_0 = (\sigma_c - \sigma_i)[\ln(\sigma^*/\sigma_c)]^{1/\lambda m^*} \quad (21)$$

where σ_c is the stress at which the change in curvature occurs. The detailed fitting procedure of the experimental log σ against log $\dot{\varepsilon}$ curves of Figs 5 and 6, to the equations presented, is described elsewhere [15, 16]. The different parameters, obtained by using a computer programme for linear regression analysis with Marquardt's method, are given in Table II. The internal stresses for all the curves of Figs 5 and 6 are shown in Fig. 7 as a function of the effective stress. The

TABLE II Parameters obtained by fitting log σ–log $\dot{\varepsilon}$ curves of Figs 5 and 6 to either Equation 2 or Equation 9

Specimen type	Temperature (K)	Σ (MPa)	σ_i (MPa)	$\dot{\varepsilon}_{J-G}/(\sigma_0)^{m^*}$ (s^{-1} MPa^{-m^*})	m^*	λ	σ^* (MPa)	$\dot{\varepsilon}_H$ (s^{-1})	σ_0 (MPa)	σ_c (MPa)	$\dot{\varepsilon}_{J-G}$ (s^{-1})
0	773	157	124	4.2×10^{-12}	3.8	0.22	123	2.5×10^{-11}	1.51	126	2.0×10^{-11}
		131	98	6.0×10^{-11}	2.6	0.19	100	2.5×10^{-11}	0.58	100	1.4×10^{-11}
		112	82	7.3×10^{-11}	2.5	0.23	81	2.1×10^{-11}	0.52	81	1.4×10^{-11}
A	773	104	84	1.3×10^{-11}	2.0	0.7	105	4.9×10^{-11}	1.94	98	4.9×10^{-11}
		52	43	3.5×10^{-11}	2.0						
B	773	113	93	4.2×10^{-12}	2.0						
		75	60	1.2×10^{-11}	1.6	0.23	84	3.5×10^{-11}	0.11	70	3.5×10^{-13}
B	823	88	23	1.2×10^{-18}	4.8	0.47	96	9.5×10^{-12}	27.4	78	9.6×10^{-12}
		67	20	4.2×10^{-17}	4.2	0.52	67	6.0×10^{-12}	16.9	56	6.0×10^{-12}
C	773	136				0.27	148	2.4×10^{-12}			
		123				0.24	133	1.6×10^{-12}			
		80	70	1.3×10^{-9}	0.42	0.49	76	1.4×10^{-12}	1.9×10^{-5}		1.3×10^{-11}
C	823	133				0.18	208	2.0×10^{-10}			
		100				0.22	128	5.5×10^{-11}			
		65				0.20	88	5.3×10^{-11}			
D	773	128	96	4.5×10^{-12}	2.3						
		93	69	3.1×10^{-12}	2.6						
D	823	121				0.22	134	8.8×10^{-12}			
		105				0.21	113	1.8×10^{-12}			
		71				0.20	77	4.1×10^{-13}			

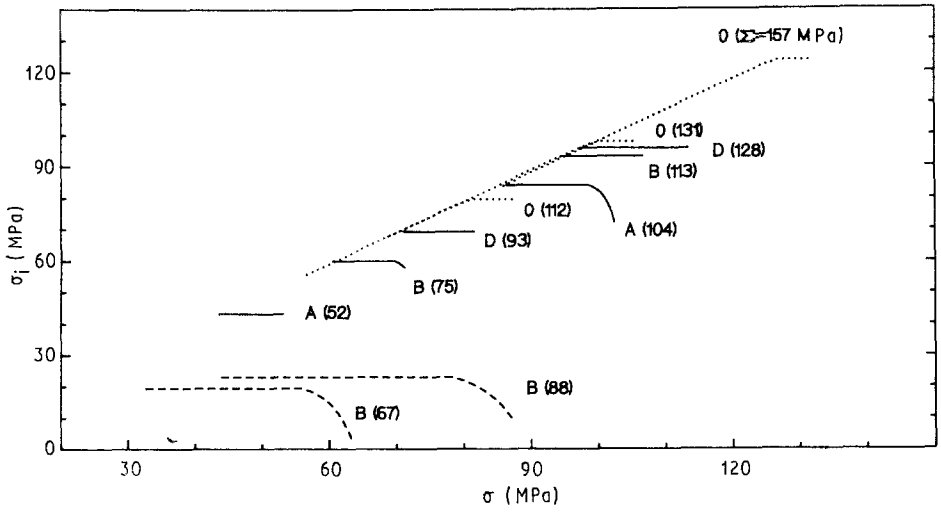

Figure 7 Internal stresses plotted against applied stress for log σ–log $\dot{\varepsilon}$ curves of Figs 5 and 6. (——) 773; (– – –) 823 K; (.....) 773 K as received.

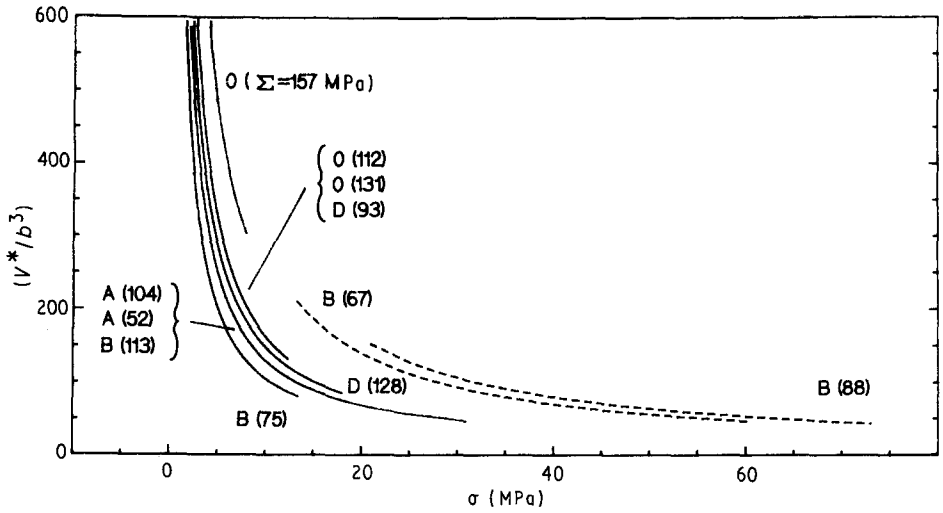

Figure 8 Activation volumes plotted against effective stress for log σ–log ε̇ curves of Figs 5 and 6. (——) 773; (– – –) 823 K.

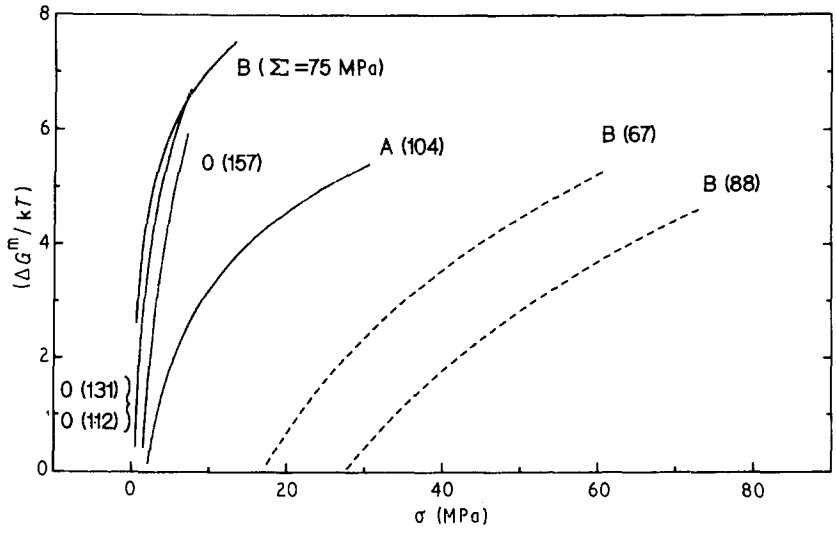

Figure 9 Free activation enthalpies plotted against effective stress for log σ–log ε̇ curves of Figs 5 and 6. (——) 773; (– – –) 823 K.

corresponding activation volumes, calculated by using either Equation 17 or 18 are shown in Fig. 8 as V^*/b^3 against $\bar{\sigma}$. Finally, plots of $\Delta G^m(\bar{\sigma})/kT$ against $\bar{\sigma}$ are shown in Fig. 9. These curves can be obtained by using either Equation 11 or 13, and the parameters given in Table II. The stress dependence of σ_i, shown in Fig. 7, should be taken into account when calculating $\Delta G^m(\bar{\sigma})$ with Equation 11. A similar calculation for the rest of the curves of Figs 5 and 6 is not possible since σ_0 cannot be determined.

4. Discussion

As pointed out in the introduction, Equation 1 can give either concave upward, linear or concave downward curves, but this equation involves too many parameters, which are very difficult to determine from the experimental curves [16]. In addition, it is not easy to give a precise physical meaning to each of the parameters in terms of thermally activated dislocation motion. A similar situation is encountered for Equation 4. The approach used in this paper, on the other hand, leads to parameters with more physical significance. Table II, however, shows that there is no clear correlation between the stress relaxation behaviour and the thermomechanical treatment given to the specimens prior to the stress relaxation experiments. This is also inferred from an observation of the stress relaxation curves given in Figs 5 and 6. To illustrate this point, Figs 10 and 11 compare the log σ–log ε̇ curves obtained at 773 and 823 K, respectively, with similar initial stresses (of the order of 100 MPa) and in specimens with different thermomechanical treatments. A*, B*, C* and D* refer to data reported in another publication [16] and correspond to the following treatments: A*, as-received + 50% cold-rolled; B*, A* + 16 h at 993 K in vacuum and air-cooled; C*, A* + 1 h at 1172 K in argon and oil-quenched + 16 h at 993 K in vacuum and air-cooled; D*, A* + 1 h at 1201 K in argon and oil-quenched + 16 h at 993 K in vacuum and air-cooled. It is evident from Fig. 10 that, except for the cold-worked specimen (indicated with A*) where a drastic difference in the stress relaxation behaviour is found with respect to the other treatments, no substantial differences are encountered between the rest of the specimens. Furthermore, it can be observed, also from Fig. 10, that similar results are obtained after the different thermal treatments, on starting from the cold-worked or from the mill-annealed condition (as received).

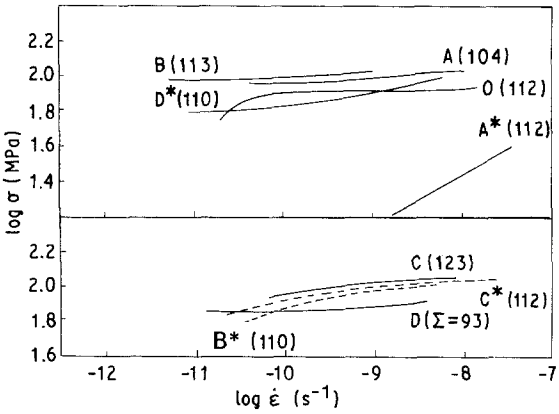

Figure 10 Stress relaxation behaviour, at 773 K, of specimens with different thermomechanical treatments and similar initial stresses. A*, B*, C* and D* indicate specimens cold-rolled before thermal treatment. A* is a 50% cold-rolled specimen.

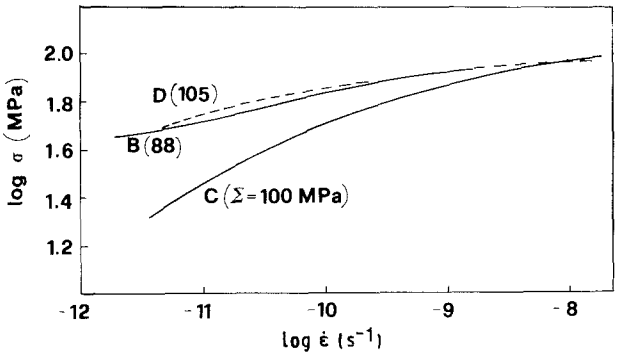

Figure 11 Stress relaxation behaviour, at 823 K, of specimens with different thermal treatments and similar initial stresses.

An interesting point is the stress dependence of the initial stresses shown in Fig. 7. When the relaxation curves are concave upward at high stresses and concave downward at low stresses, the internal stress is constant at first and then decreases as σ is reduced. This behaviour was also encountered for the load relaxation, near 563 K, of mill-annealed stainless steel type AISI 304 [15]. As shown in Fig. 7, however, a different situation is found for specimens type A and type B at 773 K, and for specimens type B at 823 K. In fact, according to Fig. 7, in these specimens and for some initial stresses, the internal stress decreases as the applied stress increases. This is due to the fact that the corresponding log σ–log $\dot{\varepsilon}$ curves show upward concavity at the lowest strain rate, as shown by Figs 5 and 6.

No specific physical model was included in the fitting procedure used in the paper, and the activation parameters obtained represent average values for the material. The large activation volumes involved, as shown in Fig. 8, and the low values for m indicate that the relaxation process is mainly due to dislocation glide controlled by the overcoming of individual solute atoms or small precipitates. In addition, thermal activation is important, since ΔG^m $(\bar{\sigma})$ is not much higher than kT, as shown in Fig. 9. A possible physical model that can be used to explain the shapes of the stress-relaxation curves and the stress dependence of the internal stresses is the occurrence of dynamic strain ageing during stress relaxation. If this is the case, it might be assumed that the effective stress is composed of three terms [23]

$$\bar{\sigma} = \sigma - \sigma_i - \sigma_s \tag{22}$$

where σ_i is an internal stress produced by the dislocation structure which does not change during stress relaxation; and σ_s the stress generated by the impurities segregated to the moving dislocation. σ_s can be expressed by

$$\sigma_s = \sigma_m\{1 - \exp[-(\dot{\varepsilon}_s/\dot{\varepsilon})^{2/(n+2)}]\} \tag{23}$$

where

$$\dot{\varepsilon}_s = (c_0/c_m)^{(n+2)/2}\alpha_n D\phi\rho(\lambda_a/b) \tag{24}$$

and

$$\sigma_m = nW_M c_m/b^3 \tag{25}$$

W_M is the binding energy between the solute atom and the dislocation, n depends on the characteristic of the interaction between the solute atom and the dislocation, D is the diffusion coefficient for the impurity, c_0 is the average concentration of impurities in the crystal, c_m is the limiting value of the concentration of impurities on the dislocation and λ_a is the average distance between the obstacles interacting with the moving dislocation.

If the stress-relaxation process is described by Equation 9, with an effective stress given by Equation 22, then

$$\dot{\varepsilon} = \frac{\dot{\varepsilon}_{J-G}}{\sigma_0^{m^*}}[(\sigma - \sigma_i - \sigma_m\{1 - \exp[-(\dot{\varepsilon}_s/\dot{\varepsilon})^{2/n+2}]\})^{m^*}] \tag{26}$$

which, on introducing

$$\frac{2}{m+2} = a \tag{27}$$

and

$$\frac{\dot{\varepsilon}_{J-G}}{\sigma_0^{m^*}} = \dot{\varepsilon}'_{J-G} \tag{28}$$

can be written as

$$\dot{\varepsilon} = \dot{\varepsilon}_{J-G}\{[\sigma - (\sigma_i + \sigma_m) + \sigma_m\exp[-(\dot{\varepsilon}_s/\dot{\varepsilon})^a]]^{m^*}\}. \tag{29}$$

Equation 29 has two limiting forms:

$$\dot{\varepsilon} = \dot{\varepsilon}'_{J-G}[\sigma - (\sigma_i + \sigma_m)]^{m^*} \quad (\dot{\varepsilon}_s \gg \dot{\varepsilon}) \tag{30}$$

and

$$\dot{\varepsilon} = \dot{\varepsilon}'_{J-G}[\sigma - \sigma_i]^{m^*} \quad (\dot{\varepsilon} \gg \dot{\varepsilon}_s) \tag{31}$$

Then, at high strain rates (high stresses) the log σ–log $\dot{\varepsilon}$ curves should be described by the Johnston–Gilman equation with an internal stress σ_i and, at low strain rates, with the same equation with an internal stress $\sigma_i + \sigma_m$. This is illustrated schematically in Fig. 12, where the limiting values are indicated by the dashed curves and the expected log σ–log $\dot{\varepsilon}$ trajectory is indicated by the full curve. The experimental curves of Figs 5 and 6 do in fact have the shape predicted by

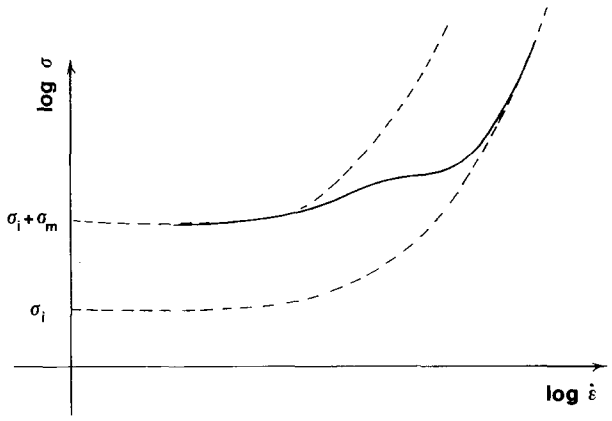

Figure 12 Schematic stress relaxation behaviour predicted by Equation 29. Broken curves represent limiting values.

Equation 29. The problem is that they are not extended enough to use the limiting values for a real determination of σ_i, σ_m and m^*. Furthermore, with the fitting procedure employed the plateau of the curve of Fig. 12 might have been used to determine σ^* and σ_i, leading to large errors, depending on how much σ_m differs from σ_i. Similar considerations apply to the value of m^* obtained experimentally, through the fitting procedure used in this paper.

Equation 29 can explain, at least qualitatively, the stress dependence of the measured internal stress, shown in Fig. 7. For specimens B (67), B(88), A(104) and B(52), a change in curvature was observed at the lowest strain rates (stresses) and so the internal stress should start to decrease with the applied stress, that is, it should change from $\sigma_i + \sigma_m$ to σ_i, according to Fig. 12. In the rest of the curves in Fig. 7, as the value of σ_i was attributed either to the plateau or to the limiting value of the lower broken curve of Fig. 12, when only concave upward curves were observed, the measured internal stress should remain constant or decrease as the applied stress is reduced. The experimental log σ–log $\dot{\varepsilon}$ curves are too short to obtain all the parameters needed for Equation 26. Some consideration should be given, however, to the parameters given in Table II. It might be assumed that curves A(52), A(52), D(128), D(93), B(113) and B(75), where the limiting stress at low strain rates is measured, give reliable values for m^*. In fact, according to Table II these curves give $m^* = 2$ for A(104) and A(52); $m^* = 2$ for B(113); and $m^* \simeq 2.4$ for D(128) and D(93). Thus, it is reasonable to assume that $m^* \simeq 2$ for all the curves in Fig. 5. Even if the experimental curves do not extend enough to obtain all the parameters of Equation 29, some estimates can be made to show that this equation might describe the log σ–log $\dot{\varepsilon}$ curves. In fact, on differentiating Equation 29 with respect to $\dot{\varepsilon}$ it can be shown that

$$\left(\frac{\dot{\varepsilon}}{\dot{\varepsilon}'_{J-G}}\right)^{1/m^*} = m^*\sigma\frac{d\log\sigma}{d\log\dot{\varepsilon}} + am^*\left(\frac{\dot{\varepsilon}_s}{\dot{\varepsilon}}\right)^a e^{-(\dot{\varepsilon}_s/\dot{\varepsilon})^a} \quad (32)$$

which, combined with Equation 29, leads to

$$\sigma\left[1 - m^*\frac{d\log\sigma}{d\log\dot{\varepsilon}}\right] = (\sigma_i + \sigma_m) + \sigma_m e^{-(\dot{\varepsilon}_s/\dot{\varepsilon})^a}\left[am^*\left(\frac{\dot{\varepsilon}_s}{\dot{\varepsilon}}\right)^a - 1\right] \quad (33)$$

For $m^* = 2$ and $n = 2$ [23], Equation 33 reduces to

$$\sigma\left[1 - \frac{1}{2}\frac{d\log\sigma}{d\log\dot{\varepsilon}}\right] = (\sigma_i + \sigma_m) + \sigma_m e^{-(\dot{\varepsilon}_s/\dot{\varepsilon})^{1/2}}\left[\left(\frac{\dot{\varepsilon}_s}{\dot{\varepsilon}}\right)^{1/2} - 1\right] \quad (34)$$

Then, for $\dot{\varepsilon} = \dot{\varepsilon}_s$, Equation 34 gives

$$\sigma\left[1 - 2\frac{d\log\sigma}{d\log\dot{\varepsilon}}\right] = (\sigma_i + \sigma_m) \quad (35)$$

Furthermore, if the experimental curve was fitted to Hart's equation in the region $\dot{\varepsilon} \simeq \dot{\varepsilon}_s$, the derivative is described by

$$\frac{d\log\sigma}{d\log\dot{\varepsilon}} = \lambda\ln(\sigma^*/\sigma) \quad (36)$$

and Equation 36 converts to

$$\sigma_1[1 - 2\lambda\ln(\sigma^*/\sigma_1)] = (\sigma_i + \sigma_m) \quad (37)$$

where σ_1 is the stress at which $\dot{\varepsilon} = \dot{\varepsilon}_s$. The values of σ_i reported in Table II do not necessarily coincide with σ_i or $\sigma_i + \sigma_m$ included in Equation 37, as the fitting procedure might lead to errors. An observation of Table II, however, shows that the ratio σ_i/Σ is constant for each specimen and it may be assumed that $(\sigma_i + \sigma_m) = K\Sigma$. For specimen B(75), $K = 0.82$, $\lambda = 0.23$, $\sigma^* = 84$ MPa, $\dot{\varepsilon}^* = 3.5 \times 10^{-11}\,s^{-1}$, $(\sigma_i + \sigma_m) = K\Sigma = 61.5$ MPa, and Equation 37 leads to $\sigma_1 = 68.1$ MPa. Once σ_1 is known, $\dot{\varepsilon}_s$ can be calculated by using Equation 2, leading to

$$\dot{\varepsilon}_s = 3.1 \times 10^{-8}\,s^{-1} \quad (38)$$

This is a reasonable value since it is located well above the saturation at $(\sigma_i + \sigma_m)$ at low strain rates, that is, the condition $\dot{\varepsilon}_s \gg \dot{\varepsilon}$ is fulfilled. In summary, it can be concluded that Equation 29 describes, not only qualitatively but also quantitatively, the experimental log σ–log $\dot{\varepsilon}$ trajectories. Data in a more extended range are needed in order to establish a correlation between the parameters given in Table II and the physical parameters involved in Equation 29. This is also valid for an evaluation of the influence of temperature on the relaxation behaviour, as no clear correlation can be established between the data at 773 K and those at 823 K. From an observation of Figs 7 and 9, it can only be concluded that the internal stresses and the activation enthalpies are lower at 823 K, indicating an acceleration of the relaxation process on increasing the temperature.

Finally, a systematic and slight increases in microhardness was observed after the stress relaxation experiments, which might be an additional confirmation that strain-ageing phenomena are occurring.

5. Conclusions

Data on stress relaxation in bending of type AISI 304 stainless steel, both at 773 and 823 K, are presented. Specimens with different thermal treatments prior to

the stress relaxation tests, and various initial stresses, were employed. The log stress against log strain rate curves were fitted to two constitutive equations, one for upward and the other one for downward concavity. Several parameters can be obtained from the experimental curves through this fitting procedure.

No clear correlation can be established between the thermal treatments and the stress relaxation behaviour, due to the influence of dynamic strain ageing. A physical model for the description of thermally activated motion of dislocations interacting with moving impurities is presented, and it is shown that this model might describe, both qualitatively and quantitatively, the observed stress relaxation behaviour.

Acknowledgements

One of the authors (F.P.) would like to thank Professor Abdus Salam, the International Atomic Energy Agency and UNESCO for hospitality at the International Centre for Theoretical Physics, Trieste, where this manuscript was completed. This work was supported partially by the Consejo Nacional de Investigaciones Cientificas y Tecnicas (CONICET) and the "Proyecto Multinacional de Investigacion y Desarrollo en Materiales" OAS–CNEA.

References

1. J. N. CONWAY, R. H. STENTZ and J. T. BERLING, "Fatigue, Tensile and Relaxation Behaviour of Stainless Steels", US Atomic Energy Commission Report TID-26135 (1975).
2. R. W. RHODE and J. C. SWEARENGEN, in Transactions of the Fourth International Conference on Structural Mechanics in Reactor Technology, Vol. L edited by A. Jaeger and B. A. Boley (North-Holland, Amsterdam, 1977) p. 85.
3. J. B. CONWAY, "An Analysis of the Relaxation Behaviour of AISI 304 and 316 Stainless Steel at Elevated Temperature", US Atomic Energy Commission Report GEMP-730 (General Electric Company, 1969).
4. E. W. HART, *Trans. J. Engng Mater. Tech.* **98** (1976) 193.
5. E. W. HART, in Transactions of the Fourth International Conference on Structural Mechanics in Reactor Technology, Vol L, edited by A. Jaeger and B. A. Boley (North-Holland, Amsterdam, 1977) p. 1/1.
6. H. YAMADA and CHE-YU LI, *Metall. Trans.* **4** (1973) 2133.
7. J. F. THOMAS Jr. and F. L. YAGGEE, *ibid.* **6A** (1975) 1835.
8. G. L. WIRE, F. V. ELLIS and CHE-YU LI, *Acta Metall.* **24** (1976) 677.
9. CHE-YU LI, F. V. ELLIS and F. H. HUANG, in "Alloys and Microstructural Design", edited by J. K. Tien and G. S. Ansell (Academic, New York, 1976) p. 403.
10. N. NIR, F. H. HUANG, E. W. HART and CHE-YU LI, *Metall. Trans.* **8A** (1977) 583.
11. F. H. HUANG, F. V. ELLIS and CHE-YU LI, *ibid.* **8A** (1977) 699.
12. H. YAMADA, *Scripta Metall.* **11** (1977) 321.
13. F. H. HUANG, H. YAMADA and CHE-YU LI, in Proceedings of the Fifth International Conference on Materials Technology, Sao Paulo (1978) p. 83.
14. M. J. ANCIAUX, *Metall. Trans.* **12A** (1981) 1981.
15. F. POVOLO and R. J. TINIVELLA, *J. Mater. Sci.* **19** (1984) 2373.
16. *Idem, ibid.* **19** (1984) 1851.
17. D. E. FRASER, P. A. ROSS-ROSS and A. R. CAUSEY, *J. Nucl. Mater.* **46** (1973) 281.
18. F. POVOLO and E. H. TOSCANO, *ibid.* **74** (1978) 76.
19. *Idem, ibid.* **78** (1978) 217.
20. L. D. BLACKBURN, in "The Generation of Isochronous Stress Strain Curves", Proceedings of the ASME Winter Annual Meeting, New York, November, 1972 (ASME, New York).
21. F. POVOLO and J. F. REGGIARDO, *J. Mater. Sci.* **23** (1988) 241.
22. W. G. JOHNSTON and J. J. GILMAN, *J. Appl. Phys.* **30** (1959) 139.
23. F. POVOLO and G. H. RUBIOLO, *Phil Mag.* **A56** (1987) 209.

Received 5 November 1990
and accepted 25 March 1991